

Supporting Information

Highly compact and smooth all-inorganic perovskite films for low threshold amplified spontaneous emission from additive-assisted solution processing

Jing Li^{†\$}, Wei Zhou^{‡\$}, Li Jiang[†], Zhishan Fang[†], Zhaoliang Yang[‡], Chen Lin[†], Xiaoli Xu^{†, #}, Zhizhen Ye[†], Haiming Zhu^{‡*}, Haiping He^{†*}

[†]State Key Laboratory of Silicon Materials, School of Materials Science and Engineering, Zhejiang University, Hangzhou 310027, P. R. China

[‡]Department of Chemistry, Zhejiang University, Hangzhou 310027, P. R. China

[#] Key Laboratory of Atomic and Molecular Physics & Functional Materials of Gansu Province, College of Physics and Electronic Engineering, Northwest Normal University, Lanzhou 730070, P. R. China

Corresponding authors: hphe@zju.edu.cn; hmzhu@zju.edu.cn

Supplementary Note 1

The grain size of Pe10 films was estimated by Scherrer equation

$$D=k\lambda/B\cos\theta, \quad (1)$$

where $k = 0.89$ is the Scherrer constant, λ is X-ray wavelength and B is the FWHM of diffraction peak. In our Pe10 films, the B values of 14.97° and 30.41° peaks are 0.148° and 0.163° respectively. The grain size is thus determined to be ~ 50 nm. The grain sizes of other films are shown in the table S1 below. It should be point out that the grain size of film deposited from mole ratio 0:100 precursor beyond the scope of the Scherrer equation, whose grain size can be estimated from SEM image directly.

Table S1 Full width at half maximum (FWHM) of XRD peaks and related grain sizes of perovskite films with various additive contents.

Mole ratios	FWHM (degree)	Grain sizes (nm)
0:100	0.13	170 (SEM)
5:100	0.13	55
10:100	0.15	50
15:100	0.20	35
20:100	0.24	28
40:100	0.33	20

Supplementary note 2

For femtosecond transient absorption spectroscopy, the fundamental output from Yb:KGW laser (1030 nm, 220 fs Gaussian fit, 100 kHz, Light Conversion Ltd) was separated to two light beam. One was introduced to NOPA (ORPHEUS-N, Light Conversion Ltd) to produce a certain wavelength for pump beam (here we use 370 nm), the other was focused onto a YAG plate to generate white light continuum as probe beam. The pump and probe overlapped on the sample at a small angle less than 10° . The transmitted probe light from sample was collected by a linear CCD array. Then we obtained transient differential transmission signals by equation shown below:

$$\frac{\Delta T}{T} = \frac{T_{pump-on} - T_{pump-off}}{T_{pump-off}} \quad (2)$$

Figure S6 shows the decay of the ground state bleaching for a pump-probe delay time after 2 ps, integrated in the wavelength range of 517-521 nm, corresponding to the population decay

of the band-edge carriers. These carriers originate from sub-picosecond relaxation of hot carriers from excitation at 370 nm. The five sets of data span the range of 4-48 $\mu\text{J cm}^{-2}$ in excitation power density. A pump intensity of 8 $\mu\text{J cm}^{-2}$ corresponding to an absorbed photon density of $1.8 \times 10^{18} \text{ cm}^{-3}$. The decay dynamics can be described by the third order equation based on free carrier model yields with universal kinetic parameters for all excitation laser power densities. The third order equation is as below:

$$\frac{dN}{dt} = -an - bn^2 - cn^3 \quad (3)$$

The global fitting yields rate constants: $a=6.18 \times 10^9$, $b=9.168 \times 10^{-9}$, $c=4 \times 10^{-28}$. The threshold of amplified stimulated emission of 14 $\mu\text{J cm}^{-2}$ at 490 nm corresponds to the carrier density of $2.74 \times 10^{18} \text{ cm}^{-3}$ covered in our energy region. It turns out that the Auger process don't dominate the decay ($an = 1.69 \times 10^{28} > cn^3 = 8.23 \times 10^{27}$) in our simulation energy region. Comparing sample 1 and sample 2, we found that there is no much difference in recombination rate and Auger rate, and it can be concluded that the main reason for low ASE threshold is not Auger rate.

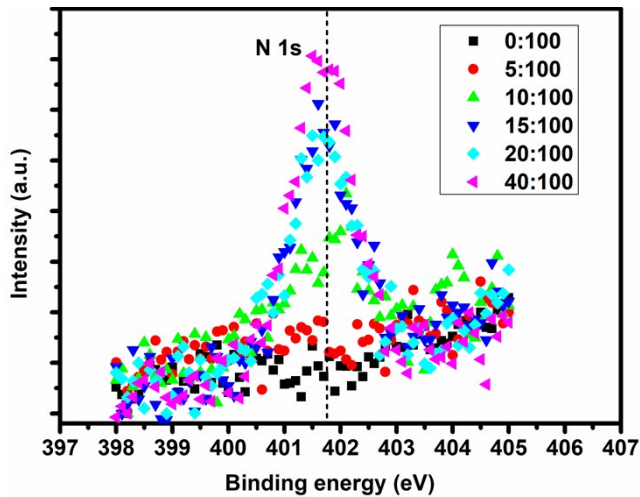


Figure S1. The N1s spectra of OABr:CsPbBr₃ films with molar ratio of 0:100, 5:100, 10:100, 15:100, 20:100, 40:100 respectively. With the increasing OABr content, the signal of N1s peak enhanced observably.

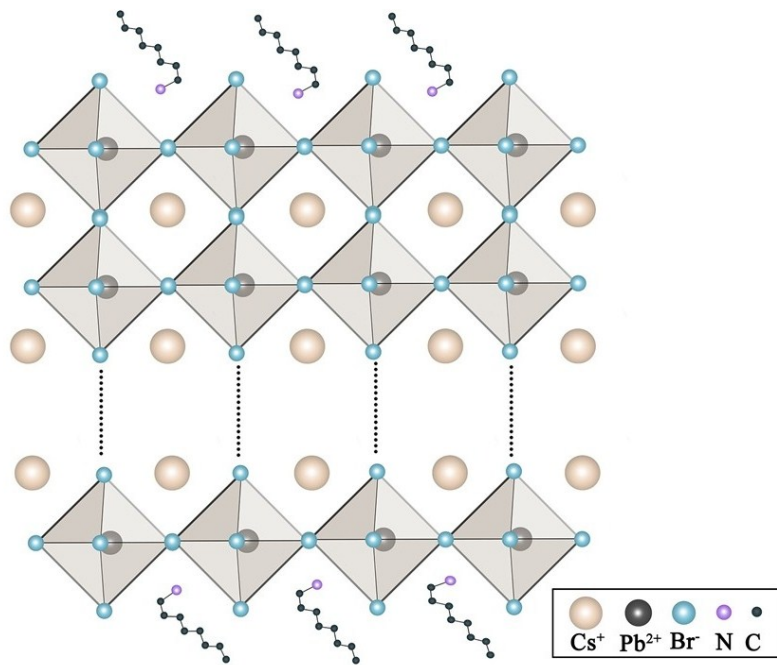


Figure S2. Schematic structure of $\text{OA}_2\text{Cs}_{n-1}\text{Pb}_n\text{Br}_{3n+1}$ perovskites.

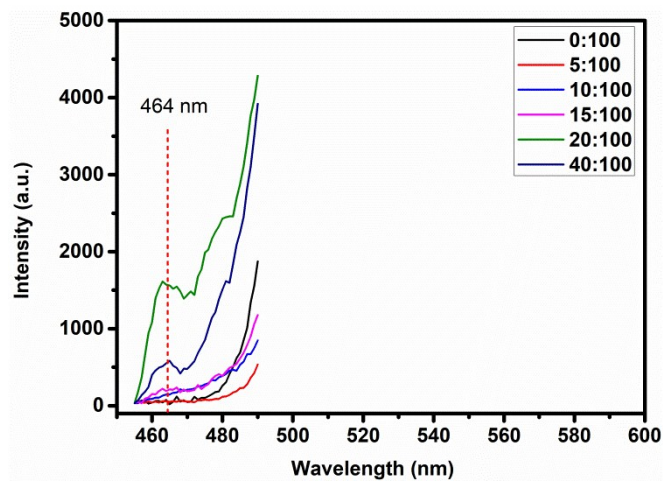


Figure S3. PL spectra of $\text{OA}\text{Br}:\text{CsPbBr}_3$ films with molar ratio of 0:100, 5:100, 10:100, 15:100, 20:100, 40:100 respectively. The low-dimensional perovskite-related emission around 464 nm appears after the adding of OABr and increases with the increase of additive ratio.

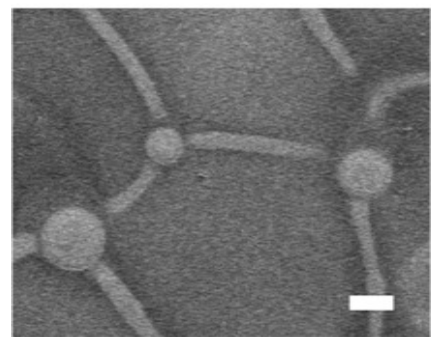


Figure S4. SEM image of the OABr-doped (40:100) CsPbBr_3 perovskite films. The spherical crystal grains are 2D perovskite structure, representing phase separation. Scale bar: 1 μm .

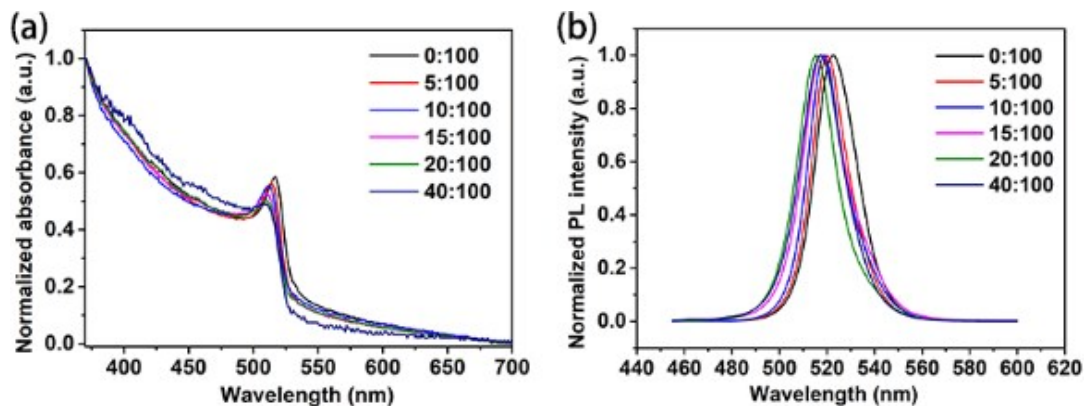


Figure S5. (a) Optical absorption and (b) PL spectra of the OABr-doped perovskite films with various molar ratios.

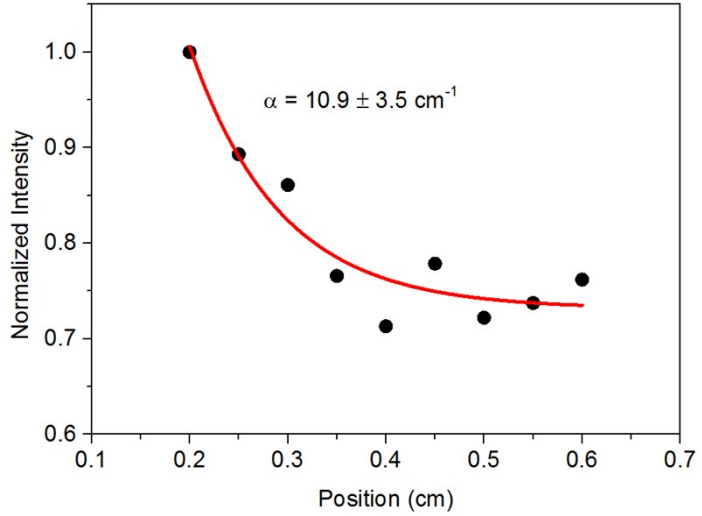


Figure S6. ASE intensity as a function of distance between the excitation stripe and detection edge. The data are fitted by $I = I_0 \exp(-\alpha d)$, where I_0 is the initial intensity, α is the loss coefficient, d is the distance. The fitting gives a loss coefficient of $10.9 \pm 3.5 \text{ cm}^{-1}$.

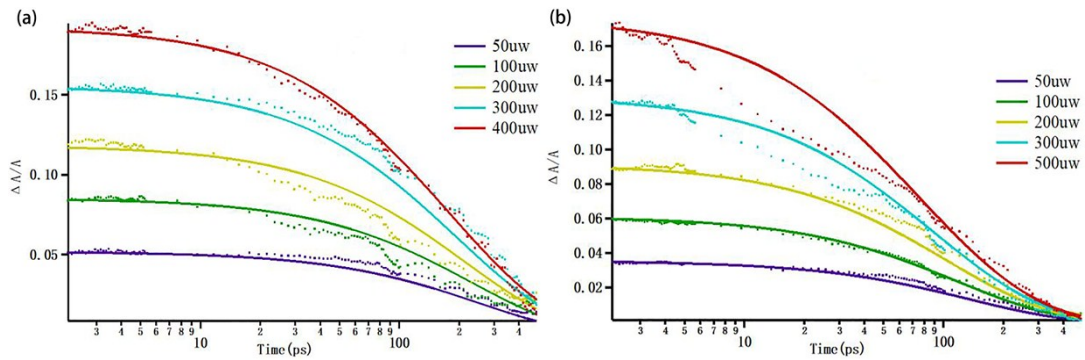


Figure S7. The femtosecond transient absorption spectroscopy of OABr-doped CsPbBr_3 films with molar ratio of (a) 0:100 and (b) 10:100 respectively. Figures show the decay of the ground state bleaching for a pump-probe delay time after 2 ps, integrated in the wavelength range of 517-521nm, corresponding to the population decay of the band-edge carriers. Solid lines are the fitting results.

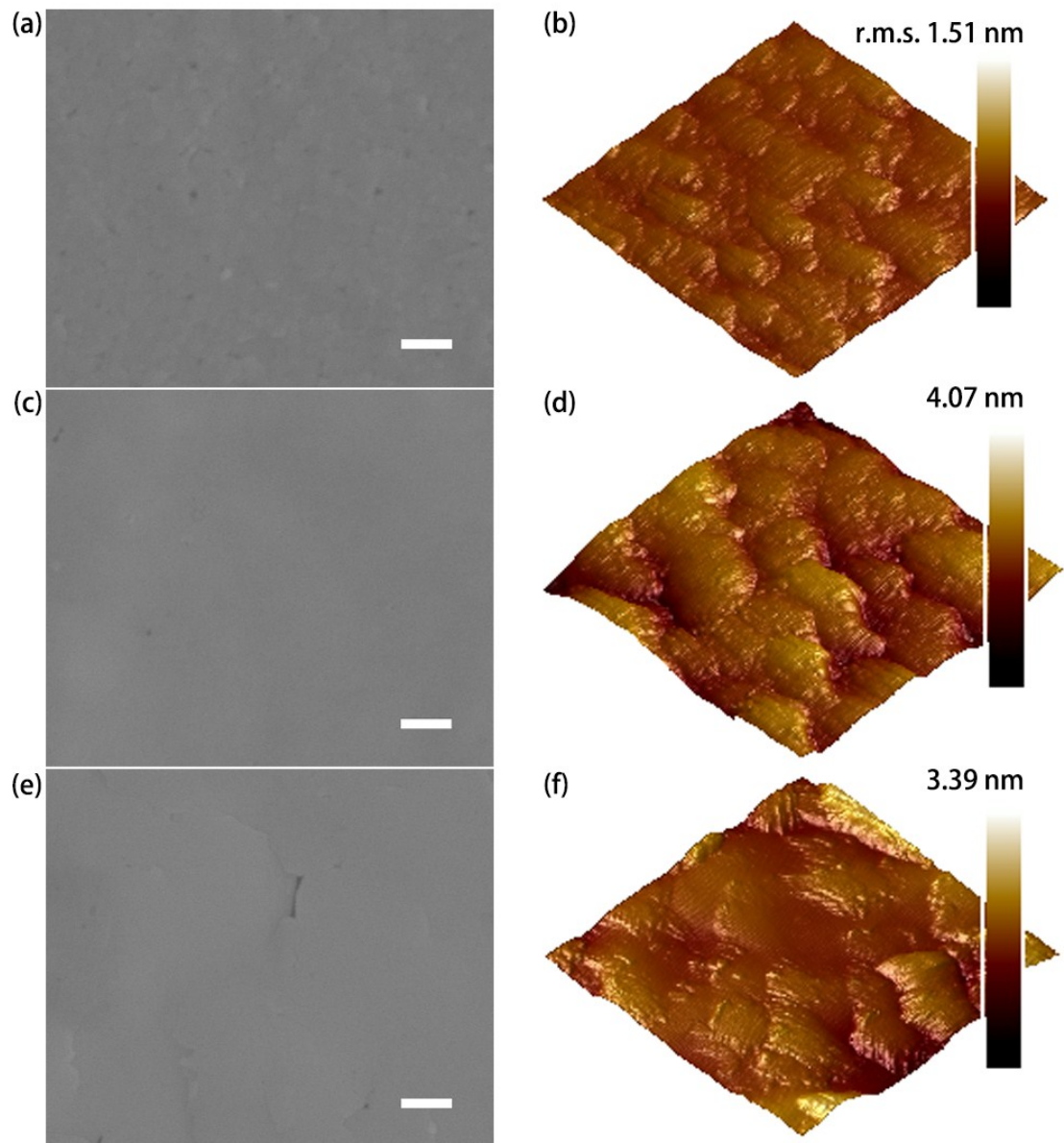


Figure S8. (a, c, e) SEM images, (b, d, f) AFM images of OABr:CsPbBr₂I, OABr:CsPbBrI₂ and OAI:CSPbI₃ thin films respectively. The SEM scale bar: 200 nm. AFM color bar: -40 to 40 nm.

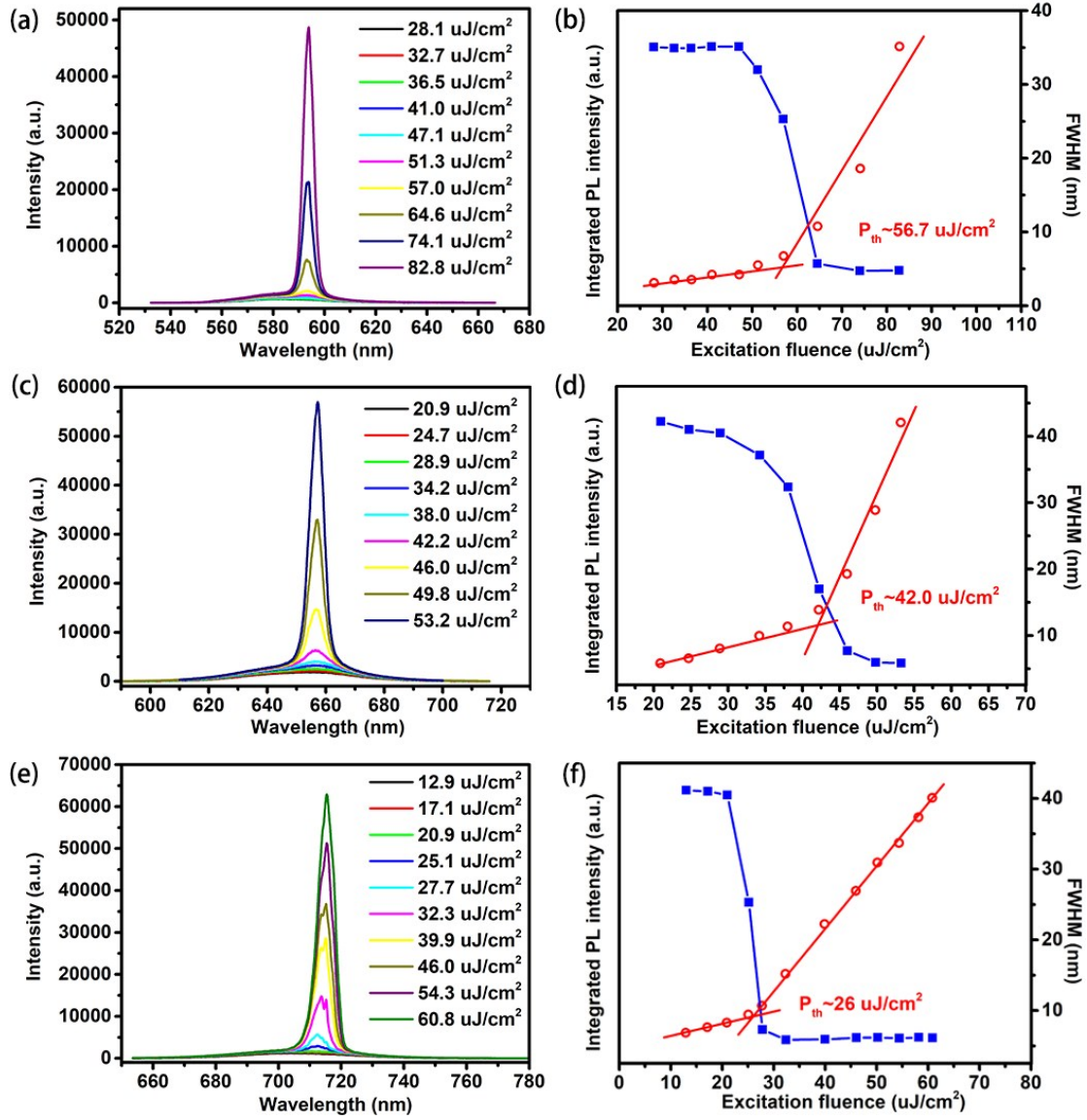


Figure S9. (a, c, e) Excitation fluence-dependent emission spectra from OABr:CsPbBr₂I, OABr:CsPbBrI₂ and OAI:CSPbI₃ thin films respectively. (b, d, f) The integrated PL intensity and FWHM vs excitation fluence of OABr:CsPbBr₂I, OABr:CsPbBrI₂ and OAI:CSPbI₃ thin films respectively.

Table S2. FWHM of the PL spectra of OABr-doped CsPbBr₃ films.

Mole ratios	FWHM (nm)
0:100	20.8
5:100	18.1
10:100	18.2
15:100	21.4
20:100	19.4
40:100	21.5

Table S3. ASE and lasing performance comparison of our OABr-doped CsPbBr₃ film with other organic-inorganic and all-inorganic perovskite films.

Material	P _{th} ^{ASE} (μJ cm ⁻²)	Gain (cm ⁻¹)	Publish Year	Ref.
MAPbI₃ Film	12	250	2014	1
MAPbI_{3-x}Cl_x Film	7.6		2015	2
MAPbI₃ Film	65	125	2014	3
MAPbI₃ Film		378	2017	4
MAPbBr₃ Film	350		2015	5
MAPbBr₃ Film	140	120	2016	6
MAPbBr₃ NWs Film	3		2016	7
MAPbBr₃ NCs Film	13.9	520	2017	8
FAPbBr₃ Film	190		2016	9
FAPbBr₃ NCs Film	14		2016	10
FAPbI₃ NCs Film	7.5		2017	11
FA_{0.1}Cs_{0.9}PbI₃ NCs Film	28		2017	11
FAPbI₃ Film	1.6		2017	12
(NMA)₂(FA)Pb₂Br₇ Film	8.5	330	2018	13
(BA)₂(MA)₅Pb₆Br₁₉ Film	13.6	112	2018	14
CsPbBr₃ NCs Film	5	450	2015	15
CsPbBr₃ NCs Film	192		2015	16
CsPbBr₃ NCs Film	22	98	2015	17
CsPbBr₃ NC Film	2.6		2016	18
CsPbBr₃ NC Film	1.5		2016	19
CsPbBr₃ NCs Film	5.6		2017	20
CsPbBr₃ Film	207		2017	21
CsPbBr₃ Film	3.17		2017	22
CsPbBr₃ Film	3.3	300	2018	23
CsSnBr_{0.5}I_{2.5} Film	7		2018	24
GAPbI₃:Tm Film	23.39		2018	25
CsPbBr₃ Film	14.9	380		This work

Table S4. Comparation of different praparation methods for all-inorganic perovskite films.

Film	Materials	Synthesis method	Roughness	Coverage	Reference
CsPbBr ₃ NCs Film	CsPbBr ₃ NC solution	Drop-casting	-	pinhole-free	15
CsPbBr ₃ NCs Film	CsPbBr ₃ QD solution	Spin-coating	-	pinhole-free	16
CsPbBr ₃ NCs Film	CsPbBr ₃ QD solution	Drop-casting	15.2 nm	pinhole-free	17
CsPbBr ₃ NC Film	CsPbBr ₃ NC solution	Drop-casting	-	pinhole-free	18
CsPbBr ₃ NC Film	CsPbBr ₃ NC solution	Spin-coating	-	pinhole-free	19
CsPbBr ₃ NCs Film	CsPbBr ₃ QD solution	Spin-coating	4.33 nm	pinhole-free	20
CsPbBr ₃ Film	CsBr/PbBr ₂ /ZnO + DMSO	One-step spin-coating	26.51 nm,	pinholes	21
CsPbBr ₃ Film	CsBr/PbBr ₂ /PEG + DMSO	One-step spin-coating	-	nearly pinhole-free	22
CsPbBr ₃ Film	CsBr/PbBr ₂	double-source thermal evaporation	2.174 nm	pinhole-free	23
CsSnBr _{0.5} I _{2.5} Film	CsI/SnBr ₂	Sequential vapor deposition	2.5 nm	pinhole-free	24
CsPbBr₃ Film	CsBr/PbBr₂/OAB + DMSO	One-step spin-coating	1.83 nm	pinhole-free	This work

References:

1. G. Xing, N. Mathews, S. S. Lim, N. Yantara, X. Liu, D. Sabba, M. Gratzel, S. Mhaisalkar and T. C. Sum, *Nat. Mater.*, 2014, **13**, 476-480.
2. S. D. Stranks, S. M. Wood, K. Wojciechowski, F. Deschler, M. Saliba, H. Khandelwal, J. B. Patel, S. J. Elston, L. M. Herz, M. B. Johnston, A. P. Schenning, M. G. Debije, M. K. Riede, S. M. Morris and H. J. Snaith, *Nano Lett.*, 2015, **15**, 4935-4941.
3. B. R. Sutherland, S. Hoogland, M. M. Adachi, C. T. O. Wong and E. H. Sargent, *ACS Nano*, 2014, **8**, 10947–10952.
4. S. Chen, C. Zhang, J. Lee, J. Han and A. Nurmikko, *Adv. Mater.*, 2017, **29**, 1604781.
5. D. Priante, I. Dursun, M. S. Alias, D. Shi, V. A. Melnikov, T. K. Ng, O. F. Mohammed, O. M. Bakr and B. S. Ooi, *Appl. Phys. Lett.* 2015, **106**, 081902.
6. J. Li, J. Si, L. Gan, Y. Liu, Z. Ye and H. He, *ACS Appl Mater Interfaces*, 2016, **8**, 32978-32983.
7. O. Vybornyi, S. Yakunin and M. V. Kovalenko, *Nanoscale*, 2016, **8**, 6278-6283.
8. S. A. Veldhuis, Y. K. E. Tay, A. Bruno, S. S. H. Dintakurti, S. Bhaumik, S. K. Muduli, M. Li, N. Mathews, T. C. Sum and S. G. Mhaisalkar, *Nano Lett.*, 2017, **17**, 7424-7432.

9. N. Arora, M. I. Dar, M. Hezam, W. Tress, G. Jacopin, T. Moehl, P. Gao, A. S. Aldwayyan, B. Deveaud, M. Grätzel and M. K. Nazeeruddin, *Adv. Funct. Mater.*, 2016, **26**, 2846-2854.
10. L. Protesescu, S. Yakunin, M. I. Bodnarchuk, F. Bertolotti, N. Masciocchi, A. Guagliardi and M. V. Kovalenko, *J. Am. Chem. Soc.*, 2016, **138**, 14202-14205.
11. L. Protesescu, S. Yakunin, S. Kumar, J. Bar, F. Bertolotti, N. Masciocchi, A. Guagliardi, M. Grotevent, I. Shorubalko, M. I. Bodnarchuk, C. J. Shih and M. V. Kovalenko, *ACS Nano*, 2017, **11**, 3119-3134.
12. F. Yuan, Z. Wu, H. Dong, J. Xi, K. Xi, G. Divitini, B. Jiao, X. Hou, S. Wang and Q. Gong, *J. Phys. Chem. C*, 2017, **121**, 15318-15325.
13. M. Li, Q. Gao, P. Liu, Q. Liao, H. Zhang, J. Yao, W. Hu, Y. Wu and H. Fu, *Adv. Funct. Mater.*, 2018, **28**, 1707006.
14. H. Zhang, Q. Liao, Y. Wu, Z. Zhang, Q. Gao, P. Liu, M. Li, J. Yao and H. Fu, *Adv. Mater.*, 2018, **30**, e1706186.
15. S. Yakunin, L. Protesescu, F. Krieg, M. I. Bodnarchuk, G. Nedelcu, M. Humer, G. De Luca, M. Fiebig, W. Heiss and M. V. Kovalenko, *Nat. Commun.*, 2015, **6**, 8056.
16. J. Pan, S. P. Sarmah, B. Murali, I. Dursun, W. Peng, M. R. Parida, J. Liu, L. Sinatra, N. Alyami, C. Zhao, E. Alarousu, T. K. Ng, B. S. Ooi, O. M. Bakr and O. F. Mohammed, *J. Phys. Chem. Lett.*, 2015, **6**, 5027-5033.
17. Y. Wang, X. Li, J. Song, L. Xiao, H. Zeng and H. Sun, *Adv. Mater.*, 2015, **27**, 7101-7108.
18. Y. Tong, E. Bladt, M. F. Ayguler, A. Manzi, K. Z. Milowska, V. A. Hintermayr, P. Docampo, S. Bals, A. S. Urban, L. Polavarapu and J. Feldmann, *Angew. Chem. Int. Ed.*, 2016, **55**, 13887-13892.
19. Q. A. Akkerman, M. Gandini, F. Di Stasio, P. Rastogi, F. Palazon, G. Bertoni, J. M. Ball, M. Prato, A. Petrozza and L. Manna, *Nat. Energy*, 2016, **2**, 16194.
20. C.-Y. Huang, C. Zou, C. Mao, K. L. Corp, Y.-C. Yao, Y.-J. Lee, C. W. Schlenker, A. K. Y. Jen and L. Y. Lin, *ACS Photonics* 2017, **4**, 2281.
21. C. Li, Z. Zang, C. Han, Z. Hu, X. Tang, J. Du, Y. Leng and K. Sun, *Nano Energy*, 2017, **40**, 195-202.
22. Z. J. Yong, Y. Zhou, J. P. Ma, Y. M. Chen, J. Y. Yang, Y. L. Song, J. Wang and H. T. Sun, *ACS Appl. Mater. Interfaces*, 2017, **9**, 32920-32929.
23. L. Zhang, F. Yuan, H. Dong, B. Jiao, W. Zhang, X. Hou, S. Wang, Q. Gong and Z. Wu, *ACS Appl. Mater. Interfaces*, 2018, **10**, 40661-40671.
24. F. Yuan, J. Xi, H. Dong, K. Xi, W. Zhang, C. Ran, B. Jiao, X. Hou, A. K. Y. Jen and Z.

- Wu, *Phys. Status Solidi RRL*, **2018**, **12**, 1800090.
25. G. M. Arumugam, C. Xu, S. K. Karunakaran, Z. Shi, F. Qin, C. Zhu and F. Chen, *J. Mater. Chem. C*, 2018, **6**, 12537-12546.